RESEARCH ARTICLE

WILEY

Distinct cerebral cortical perfusion patterns in idiopathic normal-pressure hydrocephalus

Kyunghun Kang[1] | Shin Young Jeong[2] | Ki-Su Park[3] |
Myong Hun Hahm[4] | Jaeil Kim[5] | Ho-Won Lee[1,6] | Chi-Hun Kim[7] |
Eunkyeong Yun[8] | Jaehwan Han[8] | Uicheul Yoon[8] | Sang-Woo Lee[2]

[1]Department of Neurology, School of Medicine, Kyungpook National University, Daegu, South Korea

[2]Department of Nuclear Medicine, School of Medicine, Kyungpook National University, Daegu, South Korea

[3]Department of Neurosurgery, School of Medicine, Kyungpook National University, Daegu, South Korea

[4]Department of Radiology, School of Medicine, Kyungpook National University, Daegu, South Korea

[5]School of Computer Science and Engineering, Kyungpook National University, Daegu, South Korea

[6]Brain Science and Engineering Institute, Kyungpook National University, Daegu, South Korea

[7]Department of Neurology, Hallym University Sacred Heart Hospital, Anyang, South Korea
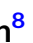
[8]Department of Biomedical Engineering, Daegu Catholic University, Gyeongsan-si, South Korea

Correspondence
Sang-Woo Lee, Department of Nuclear Medicine, School of Medicine and Chilgok Hospital, Kyungpook National University, 807 Hoguk-ro, Buk-gu, Daegu, South Korea, 41404.
Email: swleenm@knu.ac.kr

Uicheul Yoon, Department of Biomedical Engineering, Daegu Catholic University, 13-13 Hayang-Ro, Hayang-Eup, Gyeongsan-si, Gyeongbuk, South Korea, 38430.
Email: yoonuc@cu.ac.kr

Abstract

The aims of the study are to evaluate idiopathic normal-pressure hydrocephalus (INPH)-related cerebral blood flow (CBF) abnormalities and to investigate their relation to cortical thickness in INPH patients. We investigated cortical CBF utilizing surface-based early-phase ^{18}F-florbetaben (E-FBB) PET analysis in two groups: INPH patients and healthy controls. All 39 INPH patients and 20 healthy controls were imaged with MRI, including three-dimensional volumetric images, for automated surface-based cortical thickness analysis across the entire brain. A subgroup with 37 participants (22 INPH patients and 15 healthy controls) that also underwent ^{18}F-fluorodeoxyglucose (FDG) PET imaging was further analyzed. Compared with age- and gender-matched healthy controls, INPH patients showed statistically significant hyperperfusion in the high convexity of the frontal and parietal cortical regions. Importantly, within the INPH group, increased perfusion correlated with cortical thickening in these regions. Additionally, significant hypoperfusion mainly in the ventrolateral frontal cortex, supramarginal gyrus, and temporal cortical regions was observed in the INPH group relative to the control group. However, this hypoperfusion was not associated with cortical thinning. A subgroup analysis of participants that also underwent FDG PET imaging showed that increased (or decreased) cerebral perfusion was associated with increased (or decreased) glucose metabolism in INPH. A distinctive regional relationship between cerebral cortical perfusion and cortical thickness was shown in INPH patients. Our findings suggest distinct pathophysiologic mechanisms of hyperperfusion and hypoperfusion in INPH patients.

KEYWORDS
cerebral blood flow, idiopathic normal-pressure hydrocephalus, magnetic resonance imaging, positron emission tomography

Kyunghun Kang and Shin Young Jeong contributed equally to this work as first authors.

1 | INTRODUCTION

Idiopathic normal-pressure hydrocephalus (INPH) is not a common neurological disorder. Only 9 of 563 (1.6%) autopsy cases showing dementia neuropathology were suspected as INPH (Cabral et al., 2011). Even with a low incidence, diagnosing INPH is essential as INPH is widely viewed as a potentially treatable neurological disorder (Ishikawa et al., 2008). It is an adult-onset syndrome of uncertain origin involving nonobstructive enlargement of cerebral ventricles, and its symptoms are gait disturbance, cognitive impairment, and urinary dysfunction (Ishikawa et al., 2008). The cerebrospinal fluid tap test (CSFTT) is correlated with shunt effectiveness in INPH patients (Wikkelsø et al., 1982), and it is associated with a high positive predictive value for successful shunt surgery (Ishikawa et al., 2008). Under the Japanese guidelines, clinical improvement following the CSFTT increases diagnostic confidence of INPH from possible to probable (Ishikawa et al., 2008).

The cerebral vasculature may play a role in the pathogenesis of INPH (Owler & Pickard, 2001). Accordingly, several studies have examined the characteristics of cerebral blood flow (CBF) in INPH; however, the results so far have been inconsistent (Ishii et al., 2011; Ohmichi et al., 2018; Owler & Pickard, 2001; Takahashi et al., 2019; Waldemar et al., 1993). While CBF studies in INPH have not yet provided conclusive results, early reports suggest global CBF is decreased and the frontal region is most likely affected (Owler & Pickard, 2001), though, one study also reported medial frontal and parietal CBF increased in INPH patients compared with controls (Ishii et al., 2011). Another study reported that patients with INPH exhibited apparent hyperperfusion of the high convexity area on visual inspection of CBF single-photon emission computerized tomography (SPECT) images, but the presence of this sign did not indicate real hyperperfusion of the high convexity area on quantitative regional CBF analysis (Ohmichi et al., 2018). Interestingly, it was reported that the absence of regional CBF increase with an evident increase of gray matter density at the top of the high convexity might be a hallmark of INPH (Takahashi et al., 2019). However, this study included 30 INPH patients from nine different centers and 11 age-unmatched controls, and comparison between groups was performed separately for regional CBF and gray matter density (Takahashi et al., 2019). In addition, NPH was associated with an enlargement of the subcortical low flow region, a relative reduction of blood flow in the frontal cortex, and an asymmetrical reduction of regional CBF in the inferior and mid-temporal cortex, and in the central white matter (Waldemar et al., 1993). Although there was no significant difference in the cortical atrophy ratings between the control subjects and the NPH

patients, only visual inspection of computed tomographic images was performed (Waldemar et al., 1993).

Early-phase amyloid positron emission tomography (PET) images are used as a surrogate for brain perfusion (Bergeret et al., 2021). Early-phase distributions of most of the available amyloid tracers in the brain during the first minutes after injection mainly reflect regional CBF (Asghar et al., 2019). Early-phase ^{18}F-florbetaben (E-FBB) PET is also regarded as a reliable perfusion test, as validated by comparison with the gold standard Tc-99 m ethyl cysteinate dimer single photon emission tomography (Kwon et al., 2021). Generally, the blood supply to the brain is closely coupled to glucose consumption (Tiepolt et al., 2016). Further, in our recent study, E-FBB PET images showed a high correlation in ^{18}F-fluorodeoxyglucose (FDG) PET images with regard to both quantitative analyses and visual assessments (Son et al., 2020).

Recently, surface-based analysis has been applied in neuroimaging due to its effectiveness in cortical representation (Fischl et al., 1999; Park et al., 2006). One promising development in the surface-based approach is with exploring cortical thickness, which can only be mapped at the surface (Fischl & Dale, 2000; Park et al., 2006). This surface-based approach can also provide a more accurate and expansive analysis of PET images (Park et al., 2006). The surface-based analysis of CBF PET is advantageous in referencing anatomical information (i.e., cortical thickness) for a better understanding of the anatomy-perfusion relationship in INPH (Park et al., 2006). Further, an important advantage of the surface-based analysis approach is that it allows joint analysis of multiple modalities on the cortical surface, such as cortical thickness, cerebral perfusion, and cerebral metabolism (Marcoux et al., 2018).

In this study, we investigated cortical CBF utilizing surface-based E-FBB PET analysis in two groups: (1) INPH patients who had a positive response to the CSFTT and (2) healthy controls. The aims of the study are (1) to evaluate the pattern of INPH-related CBF abnormalities and (2) to investigate its relation to cortical thickness in INPH patients. In a subgroup analysis, we also explored whether an association exists between observed INPH-related CBF abnormalities and glucose metabolism in FDG PET images in INPH patients.

2 | METHODS

2.1 | Participants

Study participants were prospectively recruited from patients admitted at the Center for Neurodegenerative Diseases of Kyungpook

National University Chilgok Hospital, South Korea from May 2017 to August 2019. INPH diagnosis was made using the Relkin et al. criteria (Relkin et al., 2005). A lumbar tap extracting 30–50 ml of CSF was taken in all INPH patients. Gait changes were evaluated routinely over 7 days after the tap, and cognition and urination changes were evaluated at 1 week (Kang et al., 2013). INPH patients with a positive CSFTT response were enrolled in this study to increase diagnostic certainty. CSFTT response was defined according to three scales: Timed Up and Go (TUG) test, INPH grading scale (INPHGS), and Korean-Mini Mental State Examination (K-MMSE). The following criteria were employed to identify responders: more than 10% improvement in time on the TUG test, 1 point or more improvement on the INPHGS, or more than 3 points improvement on the K-MMSE (Kang et al., 2013).

Healthy controls were randomly chosen from our hospital and were coupled with INPH patients according to age and gender. Criteria for categorization as healthy controls were as follows: no active systemic, neurological, or psychological conditions; normal examination for neurology status; and independent functionality. Controls that were β-amyloid negative by late-phase ^{18}F-florbetaben (L-FBB) were selected. The K-MMSE was used to assess global cognition (Kang et al., 2018). The K-MMSE scores of all healthy controls were above −1.0 standard deviation of age- and education-adjusted norms.

2.2 | Neuroimaging data acquisition and analysis

2.2.1 | MRI

MRI data were gathered with a 3.0 Tesla system (GE Discovery MR750, GE Healthcare). Three-dimensional T1-weighted, sagittal, and inversion-recovery fast spoiled gradient echo (IR-FSPGR) MRI imaging of the entire head, set up to optimally distinguish brain tissues (sagittal slice thickness 1.0 mm, no gap, TR = 8.2 ms, TE = 3.2 ms, flip angle 12°, matrix size 256 × 256 pixels, and field of view = 240 mm), were attained (Kang et al., 2018).

2.2.2 | FBB PET

FBB PET images were obtained with a three-dimensional GE Discovery 600 PET/CT scanner (GE Healthcare, Milwaukee, WI). For E-FBB PET imaging, a fixed emission recording lasting 5 min (0–5 min postinjection) was started following IV injection of approximately 296 MBq FBB (Son et al., 2020). For the L-FBB PET imaging, a dynamic emission recording was used from 90 to 107 min postinjection (Son et al., 2020). A low-dose CT scan was done prior to late-phase acquisition and was used for attenuation correction in early-phase and late-phase PET data (Son et al., 2020). PET data were reconstructed with a 256 × 256 matrix, an ordered-subset expectation maximum iterative reconstruction algorithm (4 iterations; 32 subsets), and a slice thickness of 3.27 mm (Son et al., 2020). With regard to L-FBB PET, brain amyloid-β plaque load (BAPL) score was assessed based on visual ratings (Barthel et al., 2011).

A BAPL score of 1 was classified as β-amyloid negative, and BAPL scores of 2 and 3 were classified as amyloid-β positive.

2.2.3 | FDG PET

A subset of participants who consented to participating in all imaging tests also underwent FDG PET. Patients fasted for more than 6 hours, and blood glucose levels were gathered prior to FDG administration (Son et al., 2020). Patients with increased blood glucose levels more than 150 mg/dL had examinations postponed (Son et al., 2020). About 185 MBq of FDG was injected intravenously, and patients were requested to rest for 40 min in another room with dimmed light and low noise prior to undergoing FDG PET/CT imaging (Son et al., 2020). PET/CT was performed with the same scanner as FBB PET. A static emission frame was acquired from 40 to 57 min postinjection. Low-dose CT was used prior to static acquisition, and the CT scans were used for attenuation correction (Son et al., 2020). PET data were reconstructed with the same algorithm implemented for FBB PET scans.

2.2.4 | Neuroimaging data analysis

The following image processing steps were applied for analyses of cortical thickness and PET data on the cortical surface, as described in detail elsewhere (Collins et al., 1994; Lyttelton et al., 2007; MacDonald et al., 2000; Tohka et al., 2004; Van Essen et al., 2006). The native MRI data of all subjects were spatially normalized to the stereotaxic space and corrected for intensity nonuniformity artifacts (Collins et al., 1994). A hierarchical multi-scale nonlinear fitting algorithm was then applied to normalize the skull-stripped MR images by a brain extraction tool and to provide a priori information, that is, tissue probability maps for subsequent tissue classification using the neural network classifier (Collins et al., 1994). Partial volume errors (PVE) due to tissue-mixing at their interfaces were estimated and corrected using trimmed minimum covariance determinant method (Tohka et al., 2004). A maximum probability atlas defining all of the major lobes and cerebellum of the brain was warped to match each subject, and the intersection of this atlas with tissue classifications yielded cerebellar masks which would be used to calculate the standard uptake value ratio (SUVR) of PET data (Collins et al., 1994). Hemispheric cortical surfaces were automatically extracted from each MR volume using the constrained Laplacian-based automated segmentation with the proximities (CLASP) algorithm, which reconstructed the inner cortical surface by deforming a spherical mesh onto the white matter boundary and then expanded the deformable model to the gray matter boundary (MacDonald et al., 2000). Cortical thickness was measured afterward by calculating the Euclidean distance between corresponding vertices on the white matter/gray matter boundary surface and the gray matter/CSF intersection surface (MacDonald et al., 2000). Examples of spatial normalization/segmentation results of brain MRI data are given in Figure S1.

TABLE 1 Characteristics of participant samples used in analyses

	Controls versus patients			INPH patients (n = 39)		
	INPH patients	Controls	p value	L-FBB-positive INPH	L-FBB-negative INPH	p value
All participants	n = 39	n = 20		n = 11	n = 28	
Gender, male	16 (41.0)	5 (25.0)	.353	4 (36.4)	12 (42.9)	1.000
Age (year)	74.3 ± 6.9	72.0 ± 2.8	.073	78.7 ± 4.9	72.5 ± 6.9	.010
Education (year)	6.9 ± 4.7	10.6 ± 4.6	.008	7.3 ± 4.9	6.8 ± 4.8	.714
Duration of symptoms (year)	2.6 ± 2.0			2.3 ± 1.1	2.7 ± 2.2	1.000
Apolipoprotein E ε4+/ε4-	3/23			2/4	1/19	.123
K-MMSE	20.9 ± 5.7	28.2 ± 2.2	<.001	18.9 ± 8.6	21.8 ± 4.0	.315
INPHGS total	5.1 ± 1.6			5.7 ± 1.8	4.9 ± 1.5	.171
Participants who also underwent FDG PET imaging	n = 22	n = 15		n = 5	n = 17	
Gender, male	11 (50.0)	3 (20.0)	.133	2 (40.0)	9 (52.9)	1.000
Age (year)	74.5 ± 5.3	72.0 ± 3.0	.083	79.2 ± 3.1	73.1 ± 5.0	.018
Education (year)	6.0 ± 4.4	11.3 ± 4.7	.002	5.0 ± 4.8	6.2 ± 4.4	.595
Duration of symptoms (year)	2.6 ± 2.1			2.3 ± 0.8	2.6 ± 2.4	.968
Apolipoprotein E ε4+/ε4-	0/14			0/3	0/11	1.000
K-MMSE	20.0 ± 6.0	28.3 ± 2.2	<.001	15.8 ± 10.8	21.2 ± 3.3	.325
INPHGS total	5.1 ± 1.7			6.6 ± 1.8	4.7 ± 1.4	.046

Note: Values denote number (%) or mean ± *SD*.

Abbreviations: FDG, ^{18}F-fluorodeoxyglucose; INPH, idiopathic normal-pressure hydrocephalus; INPHGS, idiopathic normal-pressure hydrocephalus grading scale; K-MMSE, Korean version of mini-mental state examination; L-FBB, late-phase ^{18}F-florbetaben.

Individual E-FBB and FDG PET imaging were transformed rigidly into associated MRI scans with linear transformation from CT to MRI coregistration (Son et al., 2020). Each voxel in coregistered PET images was divided by the mean uptake of the cerebellar gray matter in each subject to form SUVR images. A cerebellar gray matter mask was generated from gray matter PVE images by retaining voxels with values greater than 0.9. Volumetric SUVR information was directly mapped to the corresponding intermediate cortical surface, halfway between the inner and outer CLASP surfaces as it represents a relatively unbiased representation of both sulcal and gyral regions, using the nearest-neighbor projection method (Van Essen et al., 2006).

We employed an iterative surface registration algorithm to ensure an optimal correspondence at each vertex of the cortical surface model across individuals (Lyttelton et al., 2007). Diffusion smoothing that generalized Gaussian kernel smoothing was used with a 30-mm full width at half maximum kernel to augment the signal-to-noise ratio and optimally detect changes in population.

All image processing results were visually inspected for quality assurance. No manual editing was performed. We excluded four subjects (one control subject and three INPH patients) due to image processing errors in brain masking, tissue classification, and cortical surface extraction.

2.3 | Statistical analyses

The surface-based statistical analysis of E-FBB PET was performed using the SurfStat toolbox (http://www.math.mcgill.ca/keith/surfstat). To analyze regional differences in SUVR between the INPH and control groups,

independent sample *t* tests were done on the surface model following matches in age and gender in the two groups. The localized regional differences in E-FBB uptake between the L-FBB-positive and L-FBB-negative INPH cases were further analyzed by applying an analysis of covariance with age, gender, disease duration, and INPHGS scores entered as covariates. Multiple comparisons were considered for the vertex data with a false discovery rate correction set at a 0.05 level of significance (p_{FDR} <.05). R version 4.0.3 (https://www.r-project.org) was also used for statistical analysis. Demographic data and average E-FBB SUVR, cortical thickness, and FDG SUVR values within all significant clusters of lower (or higher) E-FBB SUVR in INPH patients were compared between the INPH and control groups. Fisher's exact and chi-square tests were performed to compare categorical variables, and the Student's *t* test, Welch *t* tests, and Wilcoxon rank-sum tests were used to compare continuous variables. Pearson's or Spearman's correlations were used to analyze any relationships between the average E-FBB SUVR, cortical thickness, and FDG SUVR in INPH.

3 | RESULTS

The final sample for analysis was 39 INPH patients who had a positive response to the CSFTT and 20 age- and gender-matched healthy controls. Table 1 lists clinical and demographic parameters of INPH patients and control subjects. No significant differences in age and gender distribution were found between the two groups. Control subjects had statistically higher K-MMSE scores than INPH patients. Eleven of 39 INPH patients were amyloid-positive on L-FBB PET.
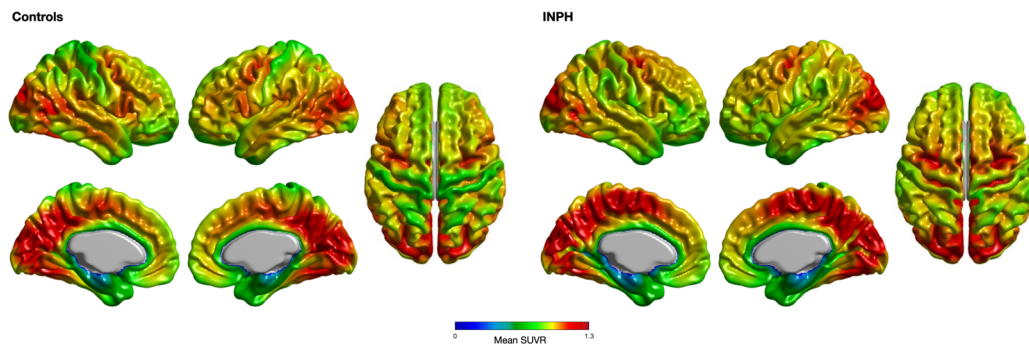
FIGURE 1 E-FBB mean images of participant groups. Surface projections are presented for healthy controls and INPH patients. E-FBB, early-phase ^{18}F-florbetaben; INPH, idiopathic normal-pressure hydrocephalus
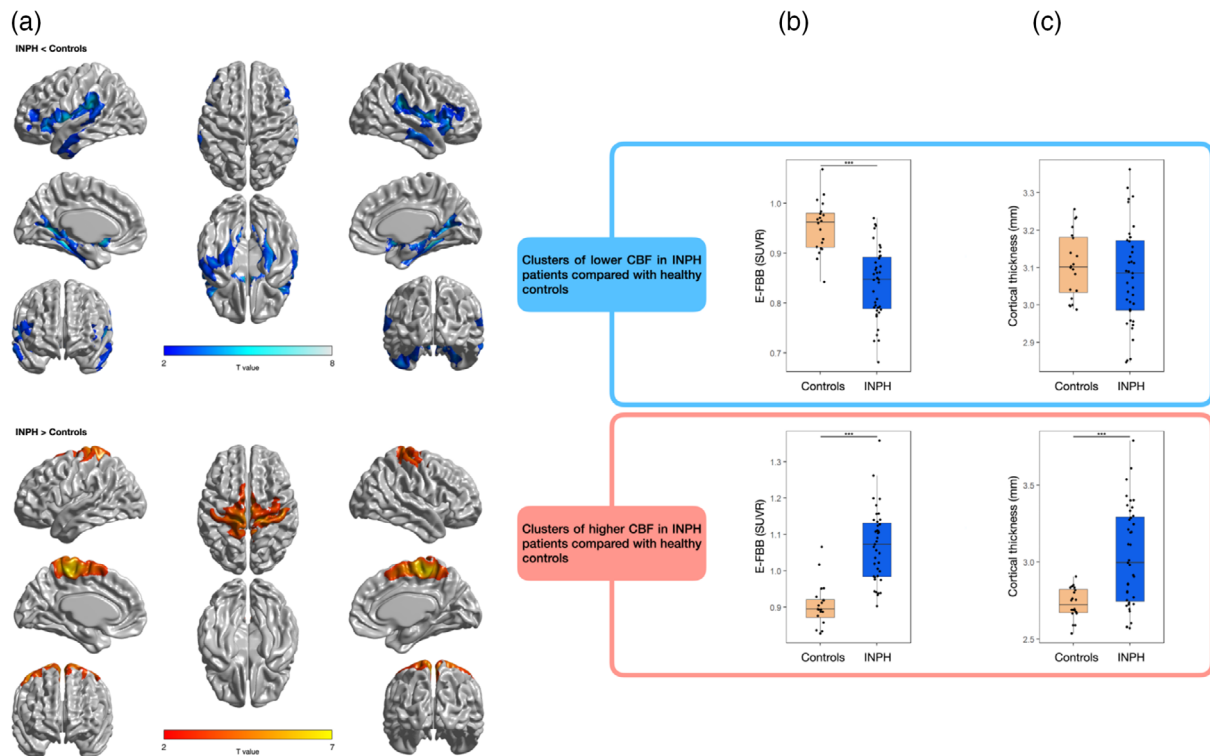

FIGURE 2 Group differences in E-FBB and cortical thickness. (a) T-maps showing the results of cortical surface-based E-FBB PET analyses. Showing lower E-FBB uptake in INPH patients when compared to healthy controls and higher E-FBB uptake in INPH patients when compared to healthy controls (p <.05, corrected for multiple comparisons with false discovery rate). Mean (b) E-FBB SUVR and (c) cortical thickness values for the brain regions with significant clusters obtained on the cortical surface-based E-FBB PET analyses in A. In clusters of higher CBF in INPH patients, INPH patients, when compared with healthy controls, showed a statistically significant increase in the average E-FBB SUVR and cortical thickness values. In clusters of lower CBF in INPH patients, INPH patients, when compared with healthy controls, showed a statistically significant decrease only in the average E-FBB SUVR values. See also Figure S2 for comparison between the L-FBB-positive and L-FBB-negative INPH cases in the average E-FBB SUVR and cortical thickness for these brain regions. CBF, cerebral blood flow; E-FBB, early-phase ^{18}F-florbetaben; INPH, idiopathic normal-pressure hydrocephalus; L-FBB, late-phase ^{18}F-florbetaben; SUVR, standardized uptake value ratio. *p <.05; **p <.01; ***p <.001

3.1 | E-FBB PET in INPH

Figure 1 shows E-FBB mean template space images for two groups. When compared to healthy controls, the INPH group revealed lower E-FBB uptake mainly in the ventrolateral frontal cortex, supramarginal gyrus, and temporal cortical regions (FDR-corrected p-value,

p_{FDR} <.05, Figure 2). The INPH group revealed higher uptake mainly in cortical regions near the high convexity of the frontal and parietal regions when compared to healthy controls (p_{FDR} <.05, Figure 2). Figure 2b shows the average E-FBB SUVR values within all significant clusters (clusters in Figure 2a) of lower (or higher) CBF in INPH patients compared with healthy controls in a box-and-whisker plot.
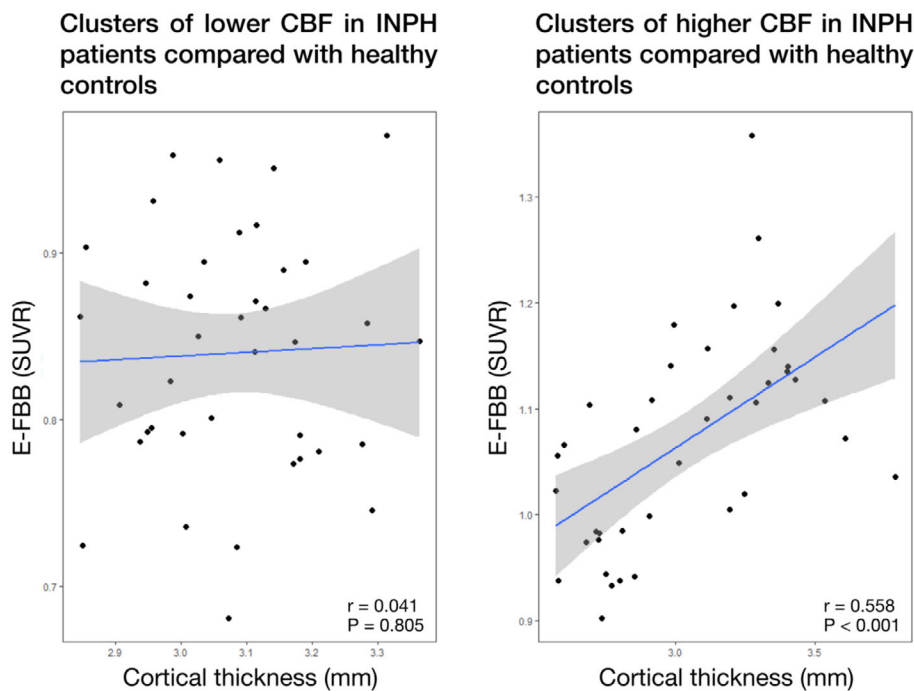
FIGURE 3 Correlations in INPH patients between mean E-FBB SUVR and cortical thickness values for the brain regions with significant clusters obtained on the cortical surface-based E-FBB PET analyses in Figure 2a. In the INPH group, the average cortical thickness correlated with the average E-FBB SUVR positively in clusters of higher CBF in INPH patients. CBF, cerebral blood flow; E-FBB, early-phase ^{18}F-florbetaben; INPH, idiopathic normal-pressure hydrocephalus; SUVR, standardized uptake value ratio

There was no significant difference in E-FBB uptake between the L-FBB-positive and L-FBB-negative subsets within the INPH group (p_{FDR} <.05).

3.2 | E-FBB and cortical thickness in INPH

Figure 2c shows the average cortical thickness values within all significant clusters (clusters in Figure 2a) of lower (or higher) CBF in INPH patients compared with healthy controls in a box-and-whisker plot. In clusters of higher CBF in INPH patients, the average cortical thickness was also significantly higher in INPH patients compared to healthy controls (p <.001). In clusters of lower CBF in INPH patients, the average cortical thickness was not significantly different between INPH patients and healthy controls.

In the INPH group, the average cortical thickness was positively correlated with the average E-FBB SUVR in clusters of higher CBF in INPH patients (Figure 3).

3.3 | E-FBB and FDG in INPH

The subgroup with participants that also underwent FDG PET imaging was further analyzed. A subset of INPH participants (n = 22) also had an FDG PET scan. This subgroup of INPH patients seemed to be demographically and cognitively representative of the whole group of patients (Table S1). No significant differences were found in age and gender distributions between the INPH and control groups. Figure 4 shows the average FDG SUVR values within all significant clusters (clusters in Figure 2a) of lower (or higher) CBF in INPH patients compared with healthy controls in a box-and-whisker plot. In clusters of

lower CBF in INPH patients, the average FDG SUVR was also significantly lower in INPH patients compared to healthy controls (p <.001). In clusters of higher CBF in INPH patients, the average FDG SUVR was also significantly higher in INPH patients compared to healthy controls (p <.001).

4 | DISCUSSION

Compared with age- and gender-matched healthy controls, INPH patients showed statistically significant hyperperfusion in the high convexity of the frontal and parietal cortical regions. Importantly, within the INPH group, increased perfusion correlated with cortical thickening in these regions. Additionally, significant hypoperfusion mainly in the ventrolateral frontal cortex, supramarginal gyrus, and temporal cortical regions was observed in the INPH group relative to the control group. However, this hypoperfusion was not associated with cortical thinning. These results provide some evidence for a characteristic pattern of cerebral perfusion changes in INPH patients.

As an explanation for the characteristic regional pattern of hyperperfusion with cortical thickening in our INPH patients, we might speculate as follows. First, hyperperfusion has been observed in patients with other neurodegenerative diseases (Dai et al., 2009; Luckhaus et al., 2008; Olm et al., 2016). A previous study using continuous arterial spin-labeling MRI reported that with regard to the Alzheimer's disease (AD) group versus control group, patients with AD had increased CBF in the right anterior cingulate gyrus (Dai et al., 2009). A previous study using contrast-enhanced perfusion-weighted MRI reported that in a subgroup analysis, dividing all mild cognitive impairment (MCI) and mild AD subjects into high versus low MMSE scorers, frontobasal hyperperfusion was observed in subjects

FIGURE 4 Mean FDG SUVR values for the brain regions with significant clusters obtained on the cortical surface-based E-FBB PET analyses in Figure 2a. In clusters of higher CBF in INPH patients, INPH patients, when compared with healthy controls, showed a statistically significant increase in average FDG SUVR values. In clusters of lower CBF in INPH patients, INPH patients, when compared with healthy controls, showed a statistically significant decrease in the average FDG SUVR values. CBF, cerebral blood flow; E-FBB, early-phase ^{18}F-florbetaben; FDG, ^{18}F-fluorodeoxyglucose; SUVR, standardized uptake value ratio. *p <.05; **p <.01; ***p <.001
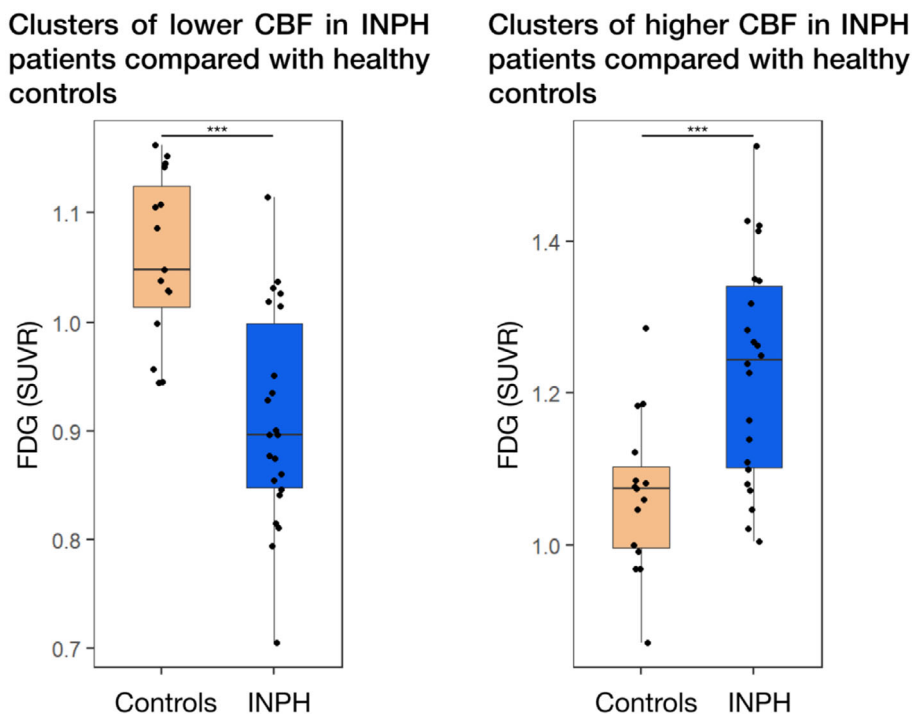
with the lower MMSE scores (Luckhaus et al., 2008). Second, in other neurodegenerative diseases, it has been suggested that hyperperfusion could be a consequence of the neuroinflammation and reactive gliosis that often follow brain pathologies (Cardenas & Bolin, 2003; Ferraro et al., 2018; Gao et al., 2013; Narayanaswami et al., 2018; Pekny & Pekna, 2016). One study reported that hyperperfusion might signal the activity enhancement of a mild diseased neural population as well as reflect neuroinflammation (Ferraro et al., 2018). Furthermore, inflammation studies in AD have reported activated microglia surrounding β-amyloid deposits within the brain that may be responsible for a locally induced inflammatory response (Salminen et al., 2009; Wilkinson et al., 2012), and hyperperfusion in AD has also been attributed to these inflammatory processes (Alsop et al., 2008; Lacalle-Aurioles et al., 2014). Reactive gliosis is well known as the cellular manifestation of neuroinflammation (Cardenas & Bolin, 2003). The dynamic and multicellular processes of neuroinflammation are mediated by the nonneuronal cells of the central nervous system, which include astrocytes and microglia (Narayanaswami et al., 2018). And reactive gliosis involves an early inflammatory response characterized by the proliferation of astrocytes and microglia following injury in the central nervous system (Gao et al., 2013). Any insult to the central nervous system tissue, including neurodegenerative diseases, also triggers reactive gliosis (Pekny & Pekna, 2016). Third, neuroinflammation and reactive gliosis are widely known to be associated with hydrocephalus (Miller & McAllister, 2007). In hydrocephalus, the stretch and compression of brain tissue caused by ventricle enlargement can cause astrocytes and microglia proliferation (Miller & McAllister, 2007). Glymphatic dysfunction is regarded as an early side-effect of neuroinflammation (Reeves et al., 2020). Neuroinflammation induced by aging or brain disease is consistently associated with a subsequent reduction in glymphatic fluid flux, possibly due to coincident reactive gliosis (Reeves et al., 2020). And human studies have implicated impaired glymphatic function in INPH (Reeves et al., 2020). Further, ventricular dilation is thought to occur at the expense of the compressible compartment as interstitial and intracellular fluids are "squeezed" out of parenchymal pores (Fattahi et al., 2016). Brain tissue compression can cause tissues to move into the nonlinear elastic regime causing stiffening (Fattahi et al., 2016). In addition, a previous MR elastography study demonstrated a unique pattern of viscoelastic alterations due to NPH, including a concentric pattern of stiffening near the dural surface and softening near the ventricles (Murphy et al., 2020). Interestingly, INPH patients demonstrated extensive surface expansion mainly in the medial aspects of the frontal horns and the superior portion of the bilateral lateral ventricles, which are surrounded by the medial frontal lobe and the high convexity of the frontal and parietal regions (Kang et al., 2018). Though INPH patients demonstrated extensive ventricular dilatation, CSF space narrowing at the high convexity and high midline areas has been conjectured to be a key imaging finding in INPH (Sasaki et al., 2008). As a consequence, these regions might be included in the main areas for the disease process in INPH. Fourth, in neurodegenerative diseases, it has been suggested that an increase in cortical thickness could be a consequence of neuroinflammation and reactive gliosis (Femminella et al., 2019; Vilaplana et al., 2020). One recent study found an association between astrocytosis, as measured by ^{11}C-deuterium-L-deprenyl PET binding, and cortical thickening in autosomal-dominant AD mutation carriers, which may suggest that astrocyte activation and corresponding hypertrophy can explain observed increases in cortical thickness (Vilaplana et al., 2020). Another recent report found a positive association between

microgliosis, as measured by translocator protein 18 kDa PET, and gray matter volume in an early MCI stage of AD, which may suggest that microglial activation is associated with cortical swelling from an early stage (Femminella et al., 2019). Consistent with our findings, a prior SPECT study on cerebral perfusion patterns in INPH patients demonstrated increased perfusion in the frontal, parietal, and occipital areas at high convexity (Ishii et al., 2011). To our knowledge, no study has simultaneously reported cerebral perfusion measurements, cortical thickness, and cerebral glucose metabolism in INPH patients. In our study, we cautiously hypothesize that hyperperfusion in INPH may result from neuroinflammation and reactive gliosis. However, the biological mechanisms producing hyperperfusion in INPH are still not fully understood, and future studies are warranted to better investigate this aspect.

As an explanation for characteristic patterns of hypoperfusion without cortical thinning in our INPH patients, we might speculate as follows. First, in neurodegenerative diseases, neuroinflammation often occurs along with the degenerative process (Garcia-Gonzalez et al., 2018). Moreover, at any given time, different brain areas are in different states (Jack Jr. et al., 2010). Second, cerebral hypoperfusion is known to be associated with neuronal degeneration (Chen et al., 2011), and is often seen in patients with INPH (Ishii et al., 2011; Momjian et al., 2004). Regarding CBF in INPH patients, many previous studies using SPECT or PET have demonstrated decreased frontal-dominant perfusion (Momjian et al., 2004). Ventriculomegaly appears to adversely affect vascular supply to specific brain regions (Del Bigio, 1993). Further, temporal lobe perfusion measured by SPECT was lower in the INPH group relative to the control group (Ishii et al., 2011). Third, in AD, it has been suggested that cerebral hypoperfusion could precede cortical thinning (Nielsen et al., 2020). A previous study using structural and perfusion-weighted MRI reported hypoperfusion, reduced blood volume, and elevated capillary transit-time heterogeneity in the parietal and frontal cortices of amyloid-positive MCI patients compared to controls, while only the precuneus showed focal cortical thinning (Nielsen et al., 2020). The study suggested further that microvascular flow disturbances might antedate cortical atrophy in amyloid-positive MCI (Nielsen et al., 2020). Additionally, aging animals that were kept for prolonged periods of time after chronic brain hypoperfusion also developed brain capillary degeneration in the CA1 hippocampus, and neuronal damage extending from the hippocampal region to the temporoparietal cortex where neurodegenerative tissue atrophy eventually formed (de la Torre, 2000). It seems therefore that as a result of cerebral hypoperfusion, brain atrophy may occur (de la Torre, 2000). Interestingly, similar to the concept of ischemic penumbra for stroke, it has been hypothesized that at least in some regions of the brain, nonatrophic hypometabolism may be the "neurodegenerative penumbra" preceding definitive cortical changes associated with atrophy (Rodriguez-Oroz et al., 2015). Considering the connection between brain perfusion and glucose metabolism, we can hypothesize that hypoperfusion without cortical thinning may also be the neurodegenerative penumbra in INPH. However, this hypothesis requires more definitive evidence in prospective longitudinal studies to determine any histopathological and biochemical basis.

A subgroup analysis of participants that also underwent FDG PET imaging showed that increased (or decreased) cerebral perfusion was associated with increased (or decreased) glucose metabolism in INPH. As mentioned above, in our previous study we reported that E-FBB PET, which reveals cerebral perfusion, correlated strongly with FDG PET, and it seems to be a valid surrogate marker for metabolic and synaptic abnormality (Son et al., 2020). Although the role of AD in patients with INPH is debated, it has been suggested that AD pathology contributes to the symptomatology of INPH and has an adverse effect on treatment outcomes (Hamilton et al., 2010). Single-session dual time-point FBB PET imaging may not only provide information on comorbid AD pathology in INPH patients but also on INPH-related CBF and metabolism abnormalities. And this might be important for diagnosis of INPH. However, these results should be interpreted cautiously due to the limited number of participants. In addition, a previous study reported that INPH patients, when compared with healthy controls, showed no specific pattern of significant cortical hypometabolism (Townley et al., 2018). However, this study was limited to only 7 participants with INPH (Townley et al., 2018).

INPH patients were selected in sequence from our INPH registry. We reduced potential bias using objective grading scales prior to and subsequently following CSFTTs as opposed to subjective accounts by patients or caregivers. Nevertheless, our study had some limitations. The first limitation was that INPH patients with a negative CSFTT response were not selected for this study to increase diagnostic certainty of INPH by limiting the analysis to CSFTT positive responders. Following the Japanese guideline, clinical improvement after the CSFTT is an important indicator that enhances diagnostic certainty from possible to probable (Ishikawa et al., 2008). However, patients with INPH in the advanced stage were also known to have a poor prognosis for treatment (Tsakanikas & Relkin, 2007). Considering the connection between the CSFTT and shunt-responsiveness (Wikkelsø et al., 1982), future studies assessing a wide sample of INPH patients in different stages of the disease would be necessary to understand the disease-stage-dependent changes of cortical CBF in INPH. The second limitation was that additional biomarkers of neuroinflammation were not tracked in our study. As a result, reactive gliosis could not be confirmed in our study participants. However, we think that there might be justification for investigating both cortical thickness and perfusion utilizing surface-based analysis in a relatively large study of INPH patients. Third, according to standards of clinical work, our PET data were acquired without arterial blood sampling. Absolute quantification of PET brain imaging requires the measurement of an arterial input function (AIF) (Sundar et al., 2019). Currently, arterial blood sampling is the standard approach for obtaining the AIF; however, this is invasive and technically challenging (Su et al., 2013). Therefore, the widely used quantification index in PET imaging is the semiquantitative SUVR, which is the ratio of radioactivity concentration of the target and reference regions (Ottoy et al., 2017). Cerebellar gray matter was used as a reference region in this study because of its low susceptibility to age-related atrophy and changes in metabolism and CBF (Ottoy et al., 2019). Furthermore, in a recent study using N-isopropyl-p-[^{123}I] iodoamphetamine and the graph plot method with

SPECT, there were no significant differences in cerebellar CBF between subjects with INPH and healthy controls (Takahashi et al., 2019). However, there is currently no genuine recommendation of guidelines for semiquantitative PET analyses in INPH. Finally, this study included a small number of healthy elderly participants because it was difficult to enroll cognitively normal elderly participants around 70 years of age with dual-phase amyloid PET and MRI. Findings from this study may encourage validation in a larger multicenter cohort.

5 | CONCLUSION

A distinctive regional relationship between cerebral cortical perfusion and cortical thickness was shown in INPH patients. INPH patients in our study had significantly increased CBF with a concomitant increase in cortical thickness in areas located in the high convexity of the frontal and parietal cortical regions in comparison to control subjects. Significantly decreased CBF without a concomitant change in cortical thickness was also observed in INPH patients relative to controls in the ventrolateral frontal cortex, supramarginal gyrus, and temporal cortical regions. Moreover, cortical areas showing hyperperfusion on E-FBB PET also showed hypermetabolism on FDG PET, and cortical areas showing hypoperfusion on E-FBB PET also showed hypometabolism on FDG PET. Our findings suggest distinct pathophysiologic mechanisms of hyperperfusion and hypoperfusion in INPH patients. Future longitudinal PET-MRI correlative studies with more participants are warranted to provide additional insights and confirm our findings.

CONFLICT OF INTEREST
The authors declare they have no competing interests.

DATA AVAILABILITY STATEMENT
The data that support the findings of this study are available upon request from the corresponding authors (S.W.L. and U.Y.). The data are not publicly available due to institute policy.

ETHICS STATEMENT
The study protocol was granted approval by the local Institutional Review Board at Kyungpook National University Chilgok Hospital. All methods and procedures were performed following specific guidelines and pertinent regulations. Each study participant gave informed and written consent to take part in the study, including information associated with clinical and imaging data. Each patient agreed to receive a CSFTT.

ORCID
Kyunghun Kang https://orcid.org/0000-0002-7248-2681
Shin Young Jeong https://orcid.org/0000-0001-5680-8314
Ki-Su Park https://orcid.org/0000-0002-4829-6299
Myong Hun Hahm https://orcid.org/0000-0001-9165-6117
Jaeil Kim https://orcid.org/0000-0002-9799-1773
Ho-Won Lee https://orcid.org/0000-0002-8849-920X
Chi-Hun Kim https://orcid.org/0000-0001-8167-4530
Uicheul Yoon https://orcid.org/0000-0002-9308-0040
Sang-Woo Lee https://orcid.org/0000-0002-7196-5366

REFERENCES
Alsop, D. C., Casement, M., de Bazelaire, C., Fong, T., & Press, D. Z. (2008). Hippocampal hyperperfusion in Alzheimer's disease. *NeuroImage*, *42*, 1267–1274.

Asghar, M., Hinz, R., Herholz, K., & Carter, S. F. (2019). Dual-phase [18F] florbetapir in frontotemporal dementia. *European Journal of Nuclear Medicine and Molecular Imaging*, *46*, 304–311.

Barthel, H., Gertz, H. J., Dresel, S., Peters, O., Bartenstein, P., Buerger, K., Hiemeyer, F., Wittemer-Rump, S. M., Seibyl, J., Reininger, C., Sabri, O., & Florbetaben Study, G. (2011). Cerebral amyloid-beta PET with florbetaben (18F) in patients with Alzheimer's disease and healthy controls: A multicentre phase 2 diagnostic study. *Lancet Neurology*, *10*, 424–435.

Bergeret, S., Queneau, M., Rodallec, M., Curis, E., Dumurgier, J., Hugon, J., Paquet, C., Farid, K., & Baron, J. C. (2021). [^{18}F]FDG PET may differentiate cerebral amyloid angiopathy from Alzheimer's disease. *European Journal of Neurology*, *28*, 1511–1519.

Cabral, D., Beach, T. G., Vedders, L., Sue, L. I., Jacobson, S., Myers, K., & Sabbagh, M. N. (2011). Frequency of Alzheimer's disease pathology at autopsy in patients with clinical normal pressure hydrocephalus. *Alzheimers Dement*, *7*, 509–513.

Cardenas, H., & Bolin, L. M. (2003). Compromised reactive microgliosis in MPTP-lesioned IL-6 KO mice. *Brain Research*, *985*, 89–97.

Chen, J. J., Rosas, H. D., & Salat, D. H. (2011). Age-associated reductions in cerebral blood flow are independent from regional atrophy. *NeuroImage*, *55*, 468–478.

Collins, D. L., Neelin, P., Peters, T. M., & Evans, A. C. (1994). Automatic 3D intersubject registration of MR volumetric data in standardized Talairach space. *Journal of Computer Assisted Tomography*, *18*, 192–205.

Dai, W., Lopez, O. L., Carmichael, O. T., Becker, J. T., Kuller, L. H., & Gach, H. M. (2009). Mild cognitive impairment and alzheimer disease: Patterns of altered cerebral blood flow at MR imaging. *Radiology*, *250*, 856–866.

de la Torre, J. C. (2000). Critically attained threshold of cerebral hypoperfusion: The CATCH hypothesis of Alzheimer's pathogenesis. *Neurobiology of Aging*, *21*, 331–342.

Del Bigio, M. R. (1993). Neuropathological changes caused by hydrocephalus. *Acta Neuropathologica*, *85*, 573–585.

Fattahi, N., Arani, A., Perry, A., Meyer, F., Manduca, A., Glaser, K., Senjem, M. L., Ehman, R. L., & Huston, J. (2016). MR Elastography demonstrates increased brain stiffness in Normal pressure hydrocephalus. *AJNR. American Journal of Neuroradiology*, *37*, 462–467.

Femminella, G. D., Dani, M., Wood, M., Fan, Z., Calsolaro, V., Atkinson, R., Edginton, T., Hinz, R., Brooks, D. J., & Edison, P. (2019). Microglial

activation in early Alzheimer trajectory is associated with higher gray matter volume. *Neurology, 92*, e1331–e1343.

Ferraro, P. M., Jester, C., Olm, C. A., Placek, K., Agosta, F., Elman, L., McCluskey, L., Irwin, D. J., Detre, J. A., Filippi, M., Grossman, M., & McMillan, C. T. (2018). Perfusion alterations converge with patterns of pathological spread in transactive response DNA-binding protein 43 proteinopathies. *Neurobiology of Aging, 68*, 85–92.

Fischl, B., & Dale, A. M. (2000). Measuring the thickness of the human cerebral cortex from magnetic resonance images. *Proceedings of the National Academy of Sciences of the United States of America, 97*, 11050–11055.

Fischl, B., Sereno, M. I., & Dale, A. M. (1999). Cortical surface-based analysis. II: Inflation, flattening, and a surface-based coordinate system. *NeuroImage, 9*, 195–207.

Gao, Z., Zhu, Q., Zhang, Y., Zhao, Y., Cai, L., Shields, C. B., & Cai, J. (2013). Reciprocal modulation between microglia and astrocyte in reactive gliosis following the CNS injury. *Molecular Neurobiology, 48*, 690–701.

Garcia-Gonzalez, P., Cabral-Miranda, F., Hetz, C., & Osorio, F. (2018). Interplay between the unfolded protein response and immune function in the development of neurodegenerative diseases. *Frontiers in Immunology, 9*, 2541.

Hamilton, R., Patel, S., Lee, E. B., Jackson, E. M., Lopinto, J., Arnold, S. E., Clark, C. M., Basil, A., Shaw, L. M., Xie, S. X., Grady, M. S., & Trojanowski, J. Q. (2010). Lack of shunt response in suspected idiopathic normal pressure hydrocephalus with Alzheimer disease pathology. *Annals of Neurology, 68*, 535–540.

Ishii, K., Hashimoto, M., Hayashida, K., Hashikawa, K., Chang, C. C., Nakagawara, J., Nakayama, T., Mori, S., & Sakakibara, R. (2011). A multicenter brain perfusion SPECT study evaluating idiopathic normal-pressure hydrocephalus on neurological improvement. *Dementia and Geriatric Cognitive Disorders, 32*, 1–10.

Ishikawa, M., Hashimoto, M., Kuwana, N., Mori, E., Miyake, H., Wachi, A., Takeuchi, T., Kazui, H., & Koyama, H. (2008). Guidelines for management of idiopathic normal pressure hydrocephalus. *Neurologia Medico-Chirurgica (Tokyo), 48*(Suppl), 1–23.

Jack, C. R., Jr., Knopman, D. S., Jagust, W. J., Shaw, L. M., Aisen, P. S., Weiner, M. W., Petersen, R. C., & Trojanowski, J. Q. (2010). Hypothetical model of dynamic biomarkers of the Alzheimer's pathological cascade. *Lancet Neurology, 9*, 119–128.

Kang, K., Kwak, K., Yoon, U., & Lee, J. M. (2018). Lateral ventricle enlargement and cortical thinning in idiopathic Normal-pressure hydrocephalus patients. *Scientific Reports, 8*, 13306.

Kang, K., Yoon, U., Lee, J. M., & Lee, H. W. (2013). Idiopathic normal-pressure hydrocephalus, cortical thinning, and the cerebrospinal fluid tap test. *Journal of the Neurological Sciences, 334*, 55–62.

Kwon, S. J., Ha, S., Yoo, S. W., Shin, N. Y., Joo Hyun, O., Yoo, I. R., & Kim, J. S. (2021). Comparison of early F-18 Florbetaben PET/CT to Tc-99m ECD SPECT using voxel, regional, and network analysis. *Scientific Reports, 11*, 16738.

Lacalle-Aurioles, M., Mateos-Pérez, J. M., Guzmán-De-Villoria, J. A., Olazarán, J., Cruz-Orduña, I., Alemán-Gómez, Y., Martino, M. E., & Desco, M. (2014). Cerebral blood flow is an earlier indicator of perfusion abnormalities than cerebral blood volume in Alzheimer's disease. *Journal of Cerebral Blood Flow and Metabolism, 34*, 654–659.

Luckhaus, C., Fluss, M. O., Wittsack, H. J., Grass-Kapanke, B., Janner, M., Khalili-Amiri, R., Friedrich, W., Supprian, T., Gaebel, W., Modder, U., & Cohnen, M. (2008). Detection of changed regional cerebral blood flow in mild cognitive impairment and early Alzheimer's dementia by perfusion-weighted magnetic resonance imaging. *NeuroImage, 40*, 495–503.

Lyttelton, O., Boucher, M., Robbins, S., & Evans, A. (2007). An unbiased iterative group registration template for cortical surface analysis. *NeuroImage, 34*, 1535–1544.

MacDonald, D., Kabani, N., Avis, D., & Evans, A. C. (2000). Automated 3-D extraction of inner and outer surfaces of cerebral cortex from MRI. *NeuroImage, 12*, 340–356.

Marcoux, A., Burgos, N., Bertrand, A., Teichmann, M., Routier, A., Wen, J., Samper-Gonzalez, J., Bottani, S., Durrleman, S., Habert, M. O., Colliot, O., Alzheimer's Disease Neuroimaging, & I. (2018). An automated pipeline for the analysis of PET data on the cortical surface. *Frontiers in Neuroinformatics, 12*, 94.

Miller, J. M., & McAllister, J. P. (2007). Reduction of astrogliosis and microgliosis by cerebrospinal fluid shunting in experimental hydrocephalus. *Cerebrospinal Fluid Research, 4*, 5.

Momjian, S., Owler, B. K., Czosnyka, Z., Czosnyka, M., Pena, A., & Pickard, J. D. (2004). Pattern of white matter regional cerebral blood flow and autoregulation in normal pressure hydrocephalus. *Brain, 127*, 965–972.

Murphy, M. C., Cogswell, P. M., Trzasko, J. D., Manduca, A., Senjem, M. L., Meyer, F. B., Ehman, R. L., & Huston, J., 3rd. (2020). Identification of Normal pressure hydrocephalus by disease-specific patterns of brain stiffness and damping ratio. *Investigative Radiology, 55*, 200–208.

Narayanaswami, V., Dahl, K., Bernard-Gauthier, V., Josephson, L., Cumming, P., & Vasdev, N. (2018). Emerging PET radiotracers and targets for imaging of Neuroinflammation in neurodegenerative diseases: Outlook beyond TSPO. *Molecular Imaging, 17*, 1536012118792317.

Nielsen, R. B., Parbo, P., Ismail, R., Dalby, R., Tietze, A., Braendgaard, H., Gottrup, H., Brooks, D. J., Ostergaard, L., & Eskildsen, S. F. (2020). Impaired perfusion and capillary dysfunction in prodromal Alzheimer's disease. *Alzheimers Dement (Amst), 12*, e12032.

Ohmichi, T., Kondo, M., Itsukage, M., Koizumi, H., Matsushima, S., Kuriyama, N., Ishii, K., Mori, E., Yamada, K., Mizuno, T., & Tokuda, T. (2018). Usefulness of the convexity apparent hyperperfusion sign in 123I-iodoamphetamine brain perfusion SPECT for the diagnosis of idiopathic normal pressure hydrocephalus. *Journal of Neurosurgery, 130*, 398–405.

Olm, C. A., Kandel, B. M., Avants, B. B., Detre, J. A., Gee, J. C., Grossman, M., & McMillan, C. T. (2016). Arterial spin labeling perfusion predicts longitudinal decline in semantic variant primary progressive aphasia. *Journal of Neurology, 263*, 1927–1938.

Ottoy, J., Verhaeghe, J., Niemantsverdriet, E., De Roeck, E., Wyffels, L., Ceyssens, S., Van Broeckhoven, C., Engelborghs, S., Stroobants, S., & Staelens, S. (2019). (18)F-FDG PET, the early phases and the delivery rate of (18)F-AV45 PET as proxies of cerebral blood flow in Alzheimer's disease: Validation against (15)O-H(2)O PET. *Alzheimers Dement, 15*, 1172–1182.

Ottoy, J., Verhaeghe, J., Niemantsverdriet, E., Wyffels, L., Somers, C., De Roeck, E., Struyfs, H., Soetewey, F., Deleye, S., Van den Bossche, T., Van Mosseveld, S., Ceyssens, S., Versijpt, J., Stroobants, S., Engelborghs, S., & Staelens, S. (2017). Validation of the Semiquantitative static SUVR method for (18)F-AV45 PET by pharmacokinetic modeling with an arterial input function. *Journal of Nuclear Medicine, 58*, 1483–1489.

Owler, B. K., & Pickard, J. D. (2001). Normal pressure hydrocephalus and cerebral blood flow: A review. *Acta Neurologica Scandinavica, 104*, 325–342.

Park, H. J., Lee, J. D., Chun, J. W., Seok, J. H., Yun, M., Oh, M. K., & Kim, J. J. (2006). Cortical surface-based analysis of 18F-FDG PET: Measured metabolic abnormalities in schizophrenia are affected by cortical structural abnormalities. *NeuroImage, 31*, 1434–1444.

Pekny, M., & Pekna, M. (2016). Reactive gliosis in the pathogenesis of CNS diseases. *Biochimica et Biophysica Acta, 1862*, 483–491.

Reeves, B. C., Karimy, J. K., Kundishora, A. J., Mestre, H., Cerci, H. M., Matouk, C., Alper, S. L., Lundgaard, I., Nedergaard, M., & Kahle, K. T. (2020). Glymphatic system impairment in Alzheimer's disease and idiopathic Normal pressure hydrocephalus. *Trends in Molecular Medicine, 26*, 285–295.

Relkin, N., Marmarou, A., Klinge, P., Bergsneider, M., & Black, P. M. (2005). Diagnosing idiopathic normal-pressure hydrocephalus. *Neurosurgery*, *57*, S4–S16.

Rodriguez-Oroz, M. C., Gago, B., Clavero, P., Delgado-Alvarado, M., Garcia-Garcia, D., & Jimenez-Urbieta, H. (2015). The relationship between atrophy and hypometabolism: Is it regionally dependent in dementias? *Current Neurology and Neuroscience Reports*, *15*, 44.

Salminen, A., Ojala, J., Kauppinen, A., Kaarniranta, K., & Suuronen, T. (2009). Inflammation in Alzheimer's disease: Amyloid-beta oligomers trigger innate immunity defence via pattern recognition receptors. *Progress in Neurobiology*, *87*, 181–194.

Sasaki, M., Honda, S., Yuasa, T., Iwamura, A., Shibata, E., & Ohba, H. (2008). Narrow CSF space at high convexity and high midline areas in idiopathic normal pressure hydrocephalus detected by axial and coronal MRI. *Neuroradiology*, *50*, 117–122.

Son, S. H., Kang, K., Ko, P. W., Lee, H. W., Lee, S. W., Ahn, B. C., Lee, J., Yoon, U., & Jeong, S. Y. (2020). Early-phase 18F-Florbetaben PET as an alternative modality for 18F-FDG PET. *Clinical Nuclear Medicine*, *45*, e8–e14.

Su, Y., Arbelaez, A. M., Benzinger, T. L., Snyder, A. Z., Vlassenko, A. G., Mintun, M. A., & Raichle, M. E. (2013). Noninvasive estimation of the arterial input function in positron emission tomography imaging of cerebral blood flow. *Journal of Cerebral Blood Flow and Metabolism*, *33*, 115–121.

Sundar, L. K., Muzik, O., Rischka, L., Hahn, A., Rausch, I., Lanzenberger, R., Hienert, M., Klebermass, E. M., Fuchsel, F. G., Hacker, M., Pilz, M., Pataraia, E., Traub-Weidinger, T., & Beyer, T. (2019). Towards quantitative [18F]FDG-PET/MRI of the brain: Automated MR-driven calculation of an image-derived input function for the non-invasive determination of cerebral glucose metabolic rates. *Journal of Cerebral Blood Flow and Metabolism*, *39*, 1516–1530.

Takahashi, R., Ishii, K., Tokuda, T., Nakajima, M., & Okada, T. (2019). Regional dissociation between the cerebral blood flow and gray matter density alterations in idiopathic normal pressure hydrocephalous: Results from SINPHONI-2 study. *Neuroradiology*, *61*, 37–42.

Tiepolt, S., Hesse, S., Patt, M., Luthardt, J., Schroeter, M. L., Hoffmann, K. T., Weise, D., Gertz, H. J., Sabri, O., & Barthel, H. (2016). Early [(18)F]florbetaben and [(11)C]PiB PET images are a surrogate biomarker of neuronal injury in Alzheimer's disease. *European Journal of Nuclear Medicine and Molecular Imaging*, *43*, 1700–1709.

Tohka, J., Zijdenbos, A., & Evans, A. (2004). Fast and robust parameter estimation for statistical partial volume models in brain MRI. *NeuroImage*, *23*, 84–97.

Townley, R. A., Botha, H., Graff-Radford, J., Boeve, B. F., Petersen, R. C., Senjem, M. L., Knopman, D. S., Lowe, V., Jack, C. R., Jr., & Jones, D. T. (2018). (18)F-FDG PET-CT pattern in idiopathic normal pressure hydrocephalus. *NeuroImage. Clinical*, *18*, 897–902.

Tsakanikas, D., & Relkin, N. (2007). Normal pressure hydrocephalus. *Seminars in Neurology*, *27*, 58–65.

Van Essen, D. C., Dierker, D., Snyder, A. Z., Raichle, M. E., Reiss, A. L., & Korenberg, J. (2006). Symmetry of cortical folding abnormalities in Williams syndrome revealed by surface-based analyses. *The Journal of Neuroscience*, *26*, 5470–5483.

Vilaplana, E., Rodriguez-Vieitez, E., Ferreira, D., Montal, V., Almkvist, O., Wall, A., Lleo, A., Westman, E., Graff, C., Fortea, J., & Nordberg, A. (2020). Cortical microstructural correlates of astrocytosis in autosomal-dominant Alzheimer disease. *Neurology*, *94*, e2026–e2036.

Waldemar, G., Schmidt, J. F., Delecluse, F., Andersen, A. R., Gjerris, F., & Paulson, O. B. (1993). High resolution SPECT with [99mTc]-d,l-HMPAO in normal pressure hydrocephalus before and after shunt operation. *Journal of Neurology, Neurosurgery, and Psychiatry*, *56*, 655–664.

Wikkelsø, C., Andersson, H., Blomstrand, C., & Lindqvist, G. (1982). The clinical effect of lumbar puncture in normal pressure hydrocephalus. *Journal of Neurology, Neurosurgery, and Psychiatry*, *45*, 64–69.

Wilkinson, B. L., Cramer, P. E., Varvel, N. H., Reed-Geaghan, E., Jiang, Q., Szabo, A., Herrup, K., Lamb, B. T., & Landreth, G. E. (2012). Ibuprofen attenuates oxidative damage through NOX2 inhibition in Alzheimer's disease. *Neurobiology of Aging*, *33*, 197.e21–e32.

SUPPORTING INFORMATION

Additional supporting information can be found online in the Supporting Information section at the end of this article.